Journal of Materials Science & Technology 57 (2020) 197–203

Contents lists available at ScienceDirect

Journal of Materials Science & Technology

journal homepage: www.jmst.org

Research Article

Exploiting ultra-large linear elasticity over a wide temperature range in nanocrystalline NiTi alloy

Zhen Sun [a], Shijie Hao [a,b,*], Genfa Kang [a], Yang Ren [c], Junpeng Liu [d], Ying Yang [a], Xiangguang Kong [a], Bo Feng [a], Cheng Wang [a], Kun Zhao [a], Lishan Cui [a]

[a] State Key Laboratory of Heavy Oil Processing, China University of Petroleum, Beijing 102249, China
[b] Beijing Key Laboratory of Failure, Corrosion, and Protection of Oil/Gas Facilities, China University of Petroleum Beijing, Beijing 102249, China
[c] X-ray Science Division, Argonne National Laboratory, Argonne, IL 60439, USA
[d] State Key Laboratory of Nonlinear Mechanics, Institute of Mechanics, Chinese Academy of Sciences, Beijing 100190, China

ARTICLE INFO

Article history:
Received 20 November 2019
Received in revised form 17 January 2020
Accepted 31 January 2020
Available online 2 June 2020

Keywords:
NiTi
Nanocrystalline
Linear-elasticity
Wide temperature range
Twinning

ABSTRACT

Many shape memory alloys can support large recoverable strains of a few percent by reversible stress-induced martensite transformation, yet they behave non-linear within a narrow operating temperature range. Developing the bulk metallic materials with ultra-large linear elasticity over a wide temperature range has proven to be difficult. In this work, a material design concept was proposed, that is true elastic deformation and reversible twinning-detwinning deformation run in parallel to overcome this challenge. By engineering the residual internal stress to realize the concurrency of true elastic deformation and twinning-detwinning deformation, a bulk nanocrystalline NiTi that possesses an ultra-large linear elastic strain up to 5.1 % and a high yield stress of 2.16 GPa over a wide temperature range of 270 °C was developed. This study offers a new avenue for developing the metallic materials with ultra-large linear elasticity over a wide temperature range of 270 °C (from 70 °C to −197 °C).

1. Introduction

Elastic strain limits of bulk metallic materials are typically less than 0.5 % due to the low critical stress for dislocation slip. It is known that the critical stress for dislocation slip can be significantly increased by multiple strengthening methods such as refinement strengthening, solution strengthening and precipitation strengthening. Nevertheless, the results obtained so far have been disappointing that the elastic strain limits of strengthened metals are always less than 2 % [1–3].

Many shape memory alloys, such as Ni-Ti and Cu-Zr-Al, can show a large reversible strain of 6 %–8 % [4–6], but it is non-linear relying on an initial elastic deformation followed by a stress-induced martensite transformation upon loading [7–9]. Although the Nb nanowires-NiTi matrix composite reported recently could exhibit a large quasi-linear elastic strain of ~6 %, its operating temperature range is fairly narrow from 15 to 50 °C [10,11], because of the strong temperature dependence of critical martensite transformation stress for NiTi matrix (the $\partial\sigma/\partial T$ is about 6 MPa/K) [12].

It is noted that similar to martensite transformation, twinning deformation is also a lattice shear at atom scale, but the critical stress for twinning deformation is insensitive to operating temperature [13–22]. It is found that in nanoscale metallic materials, the twinning deformation is reversible by combination of twinning upon loading and detwinning upon unloading due to the larger surface energy between the twinned and detwinned parts and larger back stress arising from the deformation incompatibility between twin band and grain boundary, compared with their coarse counterparts [23–29]. Unfortunately, these nanoscale metallic materials also behave a non-linear elastic deformation composed of an initial elastic deformation (stage I) and a subsequent twinning deformation (stage II) upon loading [25,26,28,29], as shown in Fig. 1(a). So far, it is a challenge to develop the bulk metallic materials exhibiting a large linear elastic deformation across a wide temperature range.

Based on the above analysis, it can be expected that a large linear elasticity with a wide temperature range may be obtained in the nanoscale metallic materials, where both the twinning deformation and elastic deformation carry on simultaneously upon tensile loading. We envisage such a case where some of the grains are in

* Corresponding author at: State Key Laboratory of Heavy Oil Processing, China University of Petroleum, Beijing 102249, China.
E-mail address: haoshijie@cup.edu.cn (S. Hao).

https://doi.org/10.1016/j.jmst.2020.01.073
1005-0302/

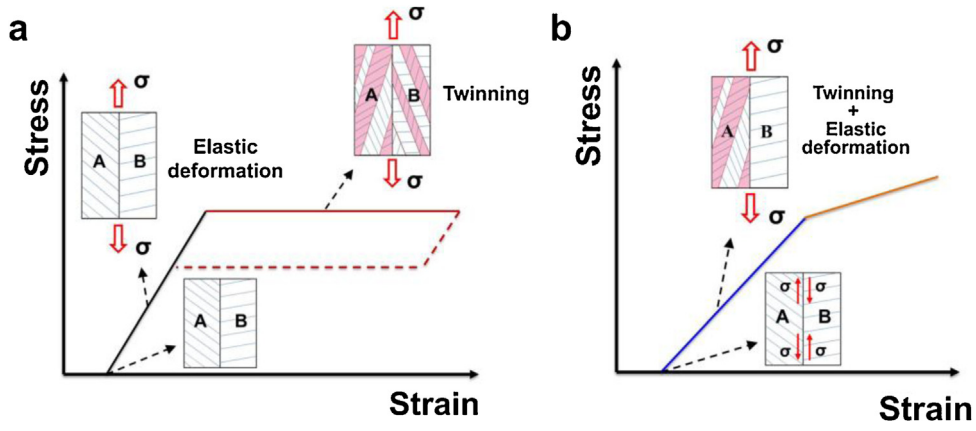

Fig. 1. Schematic of the design concept of the large linear elasticity with a wide temperature range. (a) Conventional stress-strain diagram of twinning-detwinning deformation. (b) Large linear elasticity assisted by the concurrency of elastic deformation and twinning deformation.

tension and the others are in compression before tensile loading. Upon tensile loading, the grains in tension do not undergo an initial elastic deformation, but directly produce twinning deformation, and the grains in compression undergo a large elastic deformation (consisting of preexisting elastic compression deformation and elastic tension deformation), thus presenting a large linear elasticity at macro level (shown in Fig. 1(b)). This coupling internal stress can be introduced in the nanoscale metallic materials by a specific pretreatment.

To verify this hypothesis, we fabricated a bulk nanocrystalline NiTi (NC-NiTi) using severely cold drawing followed by low temperature annealing. A high coupling internal stress was introduced in the NC-NiTi by tensile loading-unloading pre-deformation of 14 %, which makes the true elastic deformation and twinning deformation carry on simultaneously during tensile loading. The obtained NC-NiTi exhibits an ultra-large linear elastic strain of 5.1 % and high yield stress up to 2.16 GPa over a wide temperature range of 270 °C.

2. Material and methods

2.1. Materials preparation

An alloy ingot of 25 kg in weight with a composition of $Ni_{50}Ti_{50}$ (at.%) was prepared by vacuum induction melting. The raw materials used were of commercial purity Ni (99.96 wt.%) and Ti (99.90 wt.%). The ingot was hot-forged at 850 °C into a rod of 8 mm in diameter and further hot-drawn at 750 °C into a thick wire of 0.55 mm in diameter. After that, the thick wire was high-temperature annealed at 750 °C for 5 min, followed by cold-drawn into diameter of 0.29 mm at room temperature, 72 % cold deformation in cross-sectional area. The cold-drawn sample was subsequently annealed at 350 °C for 10 min followed by air cooling. The TEM bright-field image (Fig. 2(a)) presents that the annealed sample contains nanocrystallines with a mean grain size of 15 nm. The high-energy X-ray diffraction (HE-XRD) pattern in Fig. 2(b) shows that the annealed sample is B2-NiTi phase at room temperature. A tensile loading-unloading of 14 % pre-deformation was conducted on the specimen (Fig. 2(c)) at room temperature and the HE-XRD pattern (Fig. 2(d)) was indexed to B19′-NiTi phase for the pre-deformed sample. That is, B2-NiTi was transformed to B19′-NiTi and the B19′ phase was retained after unloading. The evolution of the intensity for (12), (01) and (001) planes of the B19′-NiTi phase along the Debye-Scherrer rings in the 2D HE-XRD pattern (insert of Fig. 2(d)) is shown in Fig. 2(e). The non-uniform distribution of diffraction intensity along the Debye-Scherrer rings indicates that the pre-deformed sample is composed of oriented martensitic variants. Transmission electron microscopy (TEM) bright-field image of the pre-deformed sample (shown in Fig. 2(f)) indicates that there is distinct stress contrast, meaning a high residual internal stress existing in the sample.

2.2. In-situ tensile test

In-situ synchrotron X-ray diffraction measurements were performed at the 11-IDC beamline of the Advanced Photon Source at Argonne National Laboratory. High energy X-rays of 115 keV energy and 0.6 mm × 0.6 mm beam size were used to obtain 2D diffraction patterns in the transmission geometry using a Perkin-Elmer large area detector placed at 1.8 m from the sample. The 2D diffraction patterns were collected during in-situ tensile deformation. In-situ tensile deformation was performed using an Instron testing machine at a strain rate of 5×10^{-4} s^{-1} [30] and the total elongation of the gauge length was measured with a static axial clip-on extensometer.

2.3. Microstructure and mechanical properties characterization

Microstructure of the wire was analyzed using an FEI Tecnai G^2 F20 transmission electron microscope equipped with an energy dispersive X-ray spectroscopic analyzer operated at a voltage of 200 kV. The storage modulus of the sample was measured using DMA (mechanical type: TA Q800, Dynamic Mechanical Analyzer). The DMA was set up to run a uniaxial tensile mode. During the analysis, the temperature was increased from 30 °C to to 150 °C at a rate of 5 °C /min.

3. Results and discussion

Fig. 3(a) shows the tensile stress-strain curves of the NC-NiTi tested at −197 °C and 20 °C. It is seen that the specimen exhibits a linear elastic strain up to 5.1 % and high yield stress of 2.16 GPa at −197 °C, 4.3 % and 1.42 GPa at 20 °C. Fig. 3(b) shows that the tensile loading-unloading curves at −197 °C, −100 °C, −50 °C, 20 °C and 70 °C and Fig. 3(c) presents the comparison of recovery strains between the NC-NiTi and other bulk metal materials with large elastic strains (the reversed matensite transformation temperature of the pre-deformed NC-NiTi is ~68 °C). It is obvious that the NC-NiTi possesses ultra-large linear elastic strains (4 %–5 %) across a wide temperature range of almost 270 °C (from −197 °C to 70 °C), superior to many other bulk metallic materials with large elastic strains. The ultra-large linear elastic strain and high yield strength of the NC-NiTi lead to a high mechanical energy storage density (the area under the tensile loading curve) of 53 J/cm^3 and high

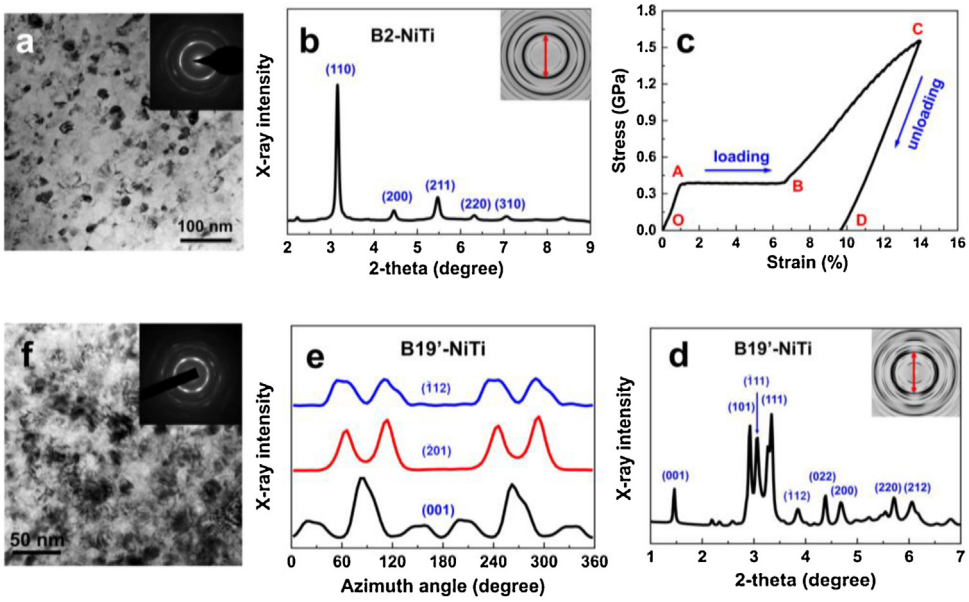

Fig. 2. Microstructures of NC-NiTi wire. (a) TEM bright-field image of annealed specimen. (b) 1D HE-XRD pattern of the annealed specimen. Insert is its corresponding 2D HE-XRD pattern. (c) 14 % tensile loading-unloading curve of the annealed specimen at 20 °C. (d) 1D HE-XRD pattern of the pre-deformed specimen. Insert is its corresponding 2D HE-XRD pattern. (e) Evolution of HE-XRD intensity for multiple planes of B19′-NiTi phase along the Debye-Scherrer rings (insert of Fig. 1(d)). (f) TEM bright-field image of the pre-deformed specimen.

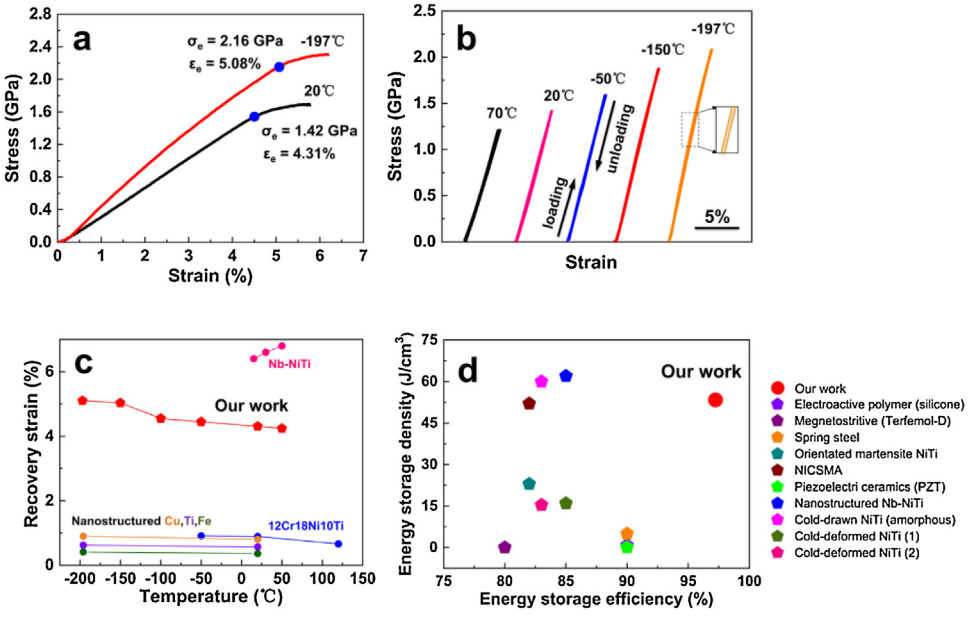

Fig. 3. Mechanical response of NC-NiTi wire. (a) Tensile stress-strain curves at −197 °C and 20 °C. (b) Tensile loading-unloading curves at −197 °C, −100 °C, −50 °C, 20 °C and 70 °C. (c) Comparison of recovery strain between the NC-NiTi and other bulk metal materials with large elastic strains [10,45,46]. (d) Comparison of mechanical energy storage density and storage efficiency between the NC-NiTi (tested at −197 °C) and other various advanced materials [10,31,47–51].

energy storage efficiency (the ratio of areas under the loading and unloading curves) of 97 %, as shown in Fig. 3(d).

To reveal the mechanism of the large linear elasticity for the NC-NiTi, in-situ HE-XRD was carried out through the tensile cycle of 4.3 % macroscopic strain. Fig. 4(a) shows the in-situ synchrotron XRD patterns of the NC-NiTi obtained over the tensile cycle. The three peaks with the highest intensity along the loading direction are (001), (002) and (03). The *d*-spacing strain of the sample along the loading direction, as determined from the B19′-NiTi (001) plane perpendicular to the loading direction, is plotted in Fig. 4(b) as a function of the macroscopic strain (the black curve). It is seen that the *d*-spacing strain is just 2.9 % when the macroscopic strain reached 4.3 % upon loading. The *d*-spacing strain of the (002) and (03) is 2.42 % and 3.71 %, respectively (shown in Fig. S1 in Supporting Information). The average *d*-spacing strain is 3.01 %. According to the mismatch between the *d*-spacing strain (3.01 %) and the macroscopic strain (4.3 %), it is believed that there is another reversible deformation involved to compensate for the macroscopic deformation. It is reported that in the martensitic NiTi with oriented variants, microtwinning appeared upon loading and disappeared upon unloading, which can offer a reversible deformation [31–34]. In the NC-NiTi, (001) compound microtwinning is the more likely to appear because of its smaller twin thickness, the lower shear strain, the lower interfacial energy and the lower strain energy compared

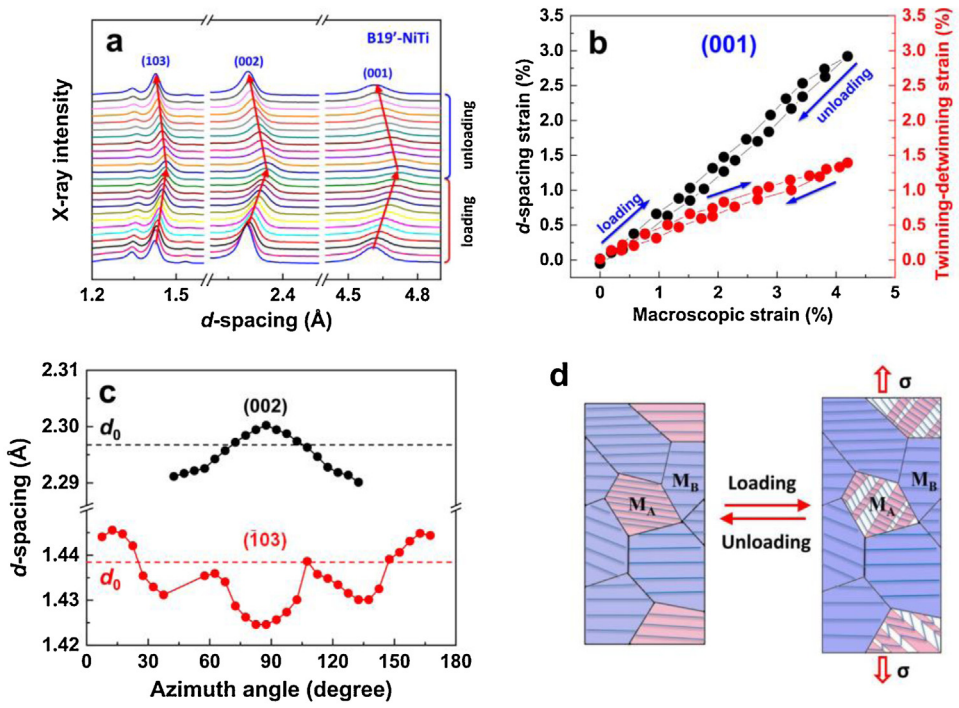

Fig. 4. (a–c) In-situ synchrotron X-ray diffraction of NC-NiTi wire at 20 °C. (a) Evolution of in-situ HE-XRD patterns during a tensile loading-unloading deformation to 4.3 % macroscopic strain. (b) The *d*-spacing strain and calculated twinning-detwinning strain with respect to macroscopic strain perpendicular to the loading direction. (c) The plot of the *d*-spacing for (002) and (03) versus the azimuthal angle, the wire longitudinal direction is 90° and the transverse direction is 0°. (d) Microstructure evolution diagram of subsequent tensile loading-unloading for the pre-deformed sample, where the pink grains are in tension and the blue ones are in compression.

with other conceivable twinning modes [35–41]. The interfacial energy and the elastic energy stored during the loading process provide the driving force for the detwinning upon unloading [23–29]. Thus it is considered that the twinning-detwinning deformation of (001) compound microtwinning was also contained in the NC-NiTi upon tensile loading and unloading.

The reversible twinning-detwinning deformation can be evaluated by the difference between macroscopic strain and *d*-spacing strain. The calculated twinning-detwinning strain (set (001) lattice plane as an example) is shown in Fig. 4(b) (the red curve) as a function of macroscopic strain. It is evident that both the *d*-spacing strain and the twinning-detwinning strain linearly increase and decrease with increasing and decreasing of the macroscopic strain throughout the tensile cycle. It is concluded that the true elastic deformation and reversible twinning-detwinning deformation run in parallel, which could contribute to the large linear elasticity of the NC-NiTi.

To uncover the reason for the concurrency of the elastic deformation and twinning deformation, the residual internal stress state of the pre-deformed sample was investigated. Fig. 4(c) shows the plot of the *d*-spacing of (002) and (03) B19′-NiTi versus the azimuthal angle. For B19′ (03), the *d*-spacing in the wire longitudinal direction (90°) is smaller than d_0, which means the grains represented by B19′ (03) are under compression in the longitudinal direction. For B19′ (002), the *d*-spacing in the wire longitudinal direction is larger than d_0, which implies that the grains represented by B19′ (002) are subjected to tensile stress in the wire longitudinal direction. During the subsequent tensile loading process (Fig. 4(d)), for the grains (such as M_A) in tension, they went through twinning deformation without the initial elastic deformation, but for the ones (such as M_B) in compression, they simply went through a large elastic deformation (consisting of preexisting elastic compression deformation and elastic tension deformation). Based on the above analysis, the concurrency of the twinning deformation and elastic deformation is ascribed to the preexisting internal tensile/compressive stresses.

Schematic representation for the formation of residual internal stress is shown in Fig. 5 (P_A and P_B represent the two grains of B2 phase, M_A and M_B represent the two grains of B19′ phase). It is considered that the annealed sample is composed of grains of different orientations (Fig. 5(a)). During the tensile loading of 14 % (shown in Fig. 2(c)), the sample underwent an initial elastic deformation of B2 phase, B2→B19′ (P→M) transformation followed by the elastic and plastic deformation of B19′ phase [42]. The grains of different orientations exhibit different phase transformation strains ($\varepsilon_{P-M}^{MA} < \varepsilon_{P-M}^{MB}$) [43], thus resulting in different elastic strains of M_A and M_B ($\varepsilon_e^A > \varepsilon_e^B$) in order to make the total strain consistent, as shown in Fig. 5(b). Upon unloading, the sample only underwent the elastic recovery of B19′ phase, where the grains (M_B) with larger phase transformation strain hindered the complete elastic recovery of the grains (M_A), leading to the internal tensile stress on M_A and compressive stress on M_B (Fig. 5(c)).

Moreover, we explored the grain size effect on the yield stress and recovery strain (pure elastic strain + twinning-detwinning strain) of the NC-NiTi. Fig. 6(a) shows the tensile loading-unloading responds of the samples with grain size of 15 nm, 50 nm, 250 nm and 350 nm at 20 °C, and Fig. 6(b) shows the corresponding statistical graph of grain size dependence of yield stress and recovery strain. It is clear that both the recovery strain and yield stress significantly increase with decreasing the grain size. The yield stress of the NC-NiTi (with mean grain size of 15 nm) is triple higher than that of its coarse counterpart (with mean grain size of 350 nm) and the recovery strain is twice larger than its coarse one. To rationalize the strong grain size dependence of yield stress and recovery strain, we analyzed the in-situ synchrotron XRD results. Fig. 6(c) shows the *d*-spacing strain (black columns) and twinning-detwinning strain (red columns) with mean grain size of 15 nm and 350 nm tested at 20 °C. It is seen that the NC-NiTi possesses a large *d*-spacing strain of 2.9 %, triple higher than 0.75 % of its coarse counterparts,

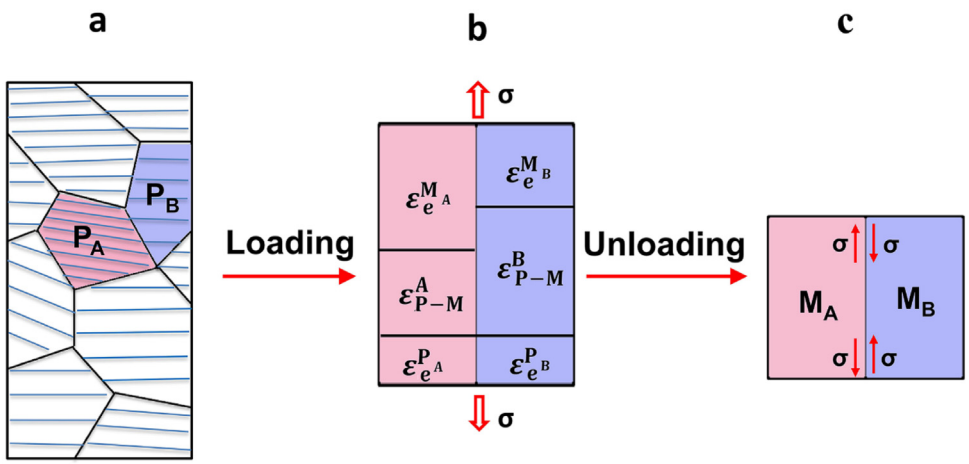

Fig. 5. Schematic representation for the formation of residual internal stress in NC-NiTi. (a) Stress-free microstructure of NC-NiTi (set P_A and P_B as the two grains of B2 phase) before pre-deformation, grains with different colors represent grains of different orientations. (b) Diagram of tensile loading of 14 %, where $\varepsilon_{P-M}^{A} < \varepsilon_{P-M}^{B}$, $\varepsilon_e^{MA} > \varepsilon_e^{MB}$. (c) Stress states of the two grains inside NC-NiTi (set M_A and M_B as the two grains of B19′ phase) after unloaded, where the red arrows represent the direction of internal stress.

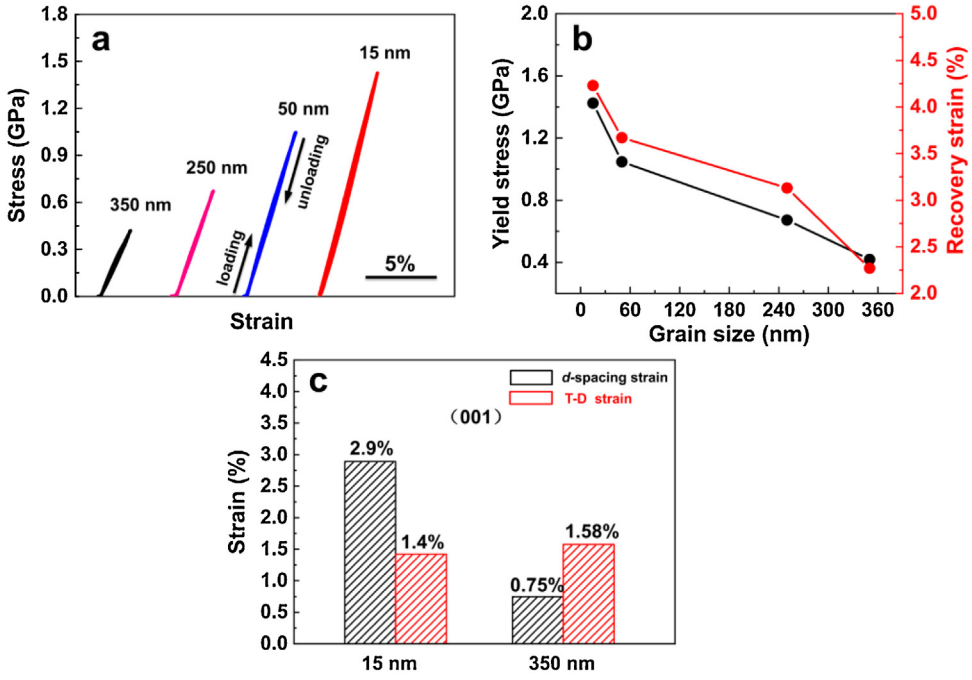

Fig. 6. Linear elastic mechanical characteristics of the NiTi samples with varying mean grain sizes between 15 nm and 350 nm at 20 °C. (a) Tensile loading-unloading curves. (b) Grain-size dependence of yield stress and recovery strain. (c) Comparison of *d*-spacing strain and twinning-detwinning strain.

the same trend as the yield stress discussed above. We can draw a conclusion that the higher yield stress attributes to the intrinsic larger elastic strain (interatomic spacing strain) of the NC-NiTi than its coarse counterpart, according to the Hooke's law. Besides that, the larger recovery strain of NC-NiTi also attributes to the intrinsic larger elastic strain, because of the sub-equal twinning-detwinning strain between the NC-NiTi (1.4 %) and its coarse one (1.58 %).

The testing temperature effect on the yield stress and recovery strain of the samples with different grain sizes are also investigated. Fig. 7(a) presents the yield stress of the samples with mean grain size of 15 nm and 350 nm as a function of the testing temperature. It is obvious that the yield stress of the NC-NiTi increases by more than 600 MPa triple higher than 200 MPa of its coarse counterparts, when the testing temperature decreases from 70 °C to −150 °C. To rationalize the strong temperature effect on yield stress for the NC-NiTi, we analyzed the dynamic mechanical analyzer (Fig. 7 (c)) and in-situ synchrotron XRD (Fig. 7 (d)) results. Fig. 7 (c) shows that the storage modulus (positively relevant to the elastic modulus, thus simply regarded as elastic modulus here) normalized by the initial value of NC-NiTi significantly increases faster than that of its coarse counterpart with decreasing the testing temperature. This attributes to the fact that the elastic modulus of grain boundary is more temperature-sensitive, where the grain boundary shows more local deformation compared with the grain core component under a slight thermal fluctuations [44]. Fig. 7 (d) shows the *d*-spacing strain and twinning-detwinning strain with mean grain size of 15 nm and 350 nm tested at 20 °C and −100 °C, respectively. It is seen that the *d*-spacing strain declines slightly from 2.9 % to 2.6 % of NC-NiTi (the same trend for the coarse one), within the temperature range from 20 °C to −100 °C. Thus, it is expected that the more rapid increase of yield stress of the NC-NiTi originates from

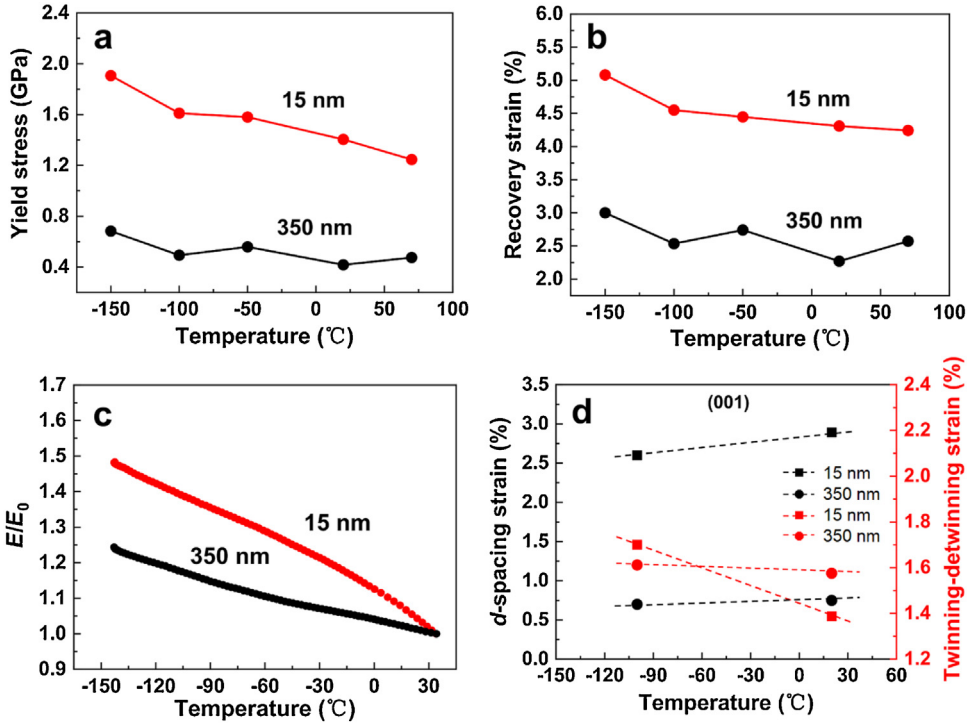

Fig. 7. Linear elastic mechanical characteristics of the NiTi with mean grain size of 15 nm and 350 nm from −150 °C to 70 °C. Testing temperature effect on (a) yield stress as well as (b) recovery strain. (c) Storage modulus change as a function of testing temperature. (d) Testing temperature effect on *d*-spacing strain and twinning-detwinning strain.

the faster increase of elastic modulus with decreasing temperature, compared with its coarse counterpart.

Fig. 7 (b) shows the recovery strain of the samples with mean grain size of 15 nm and 350 nm as a function of the testing temperature. It is seen that the recovery strains of the two samples slowly increase with decreasing the testing temperature. Fig. 7 (d) shows that the *d*-spacing strains of the two samples slightly decrease and the twinning-detwinning strains slowly increase with decreasing the testing temperature. It is considered that the descending in the *d*-spacing strains may stem from the increase of elastic modulus with decreasing the testing temperature (Fig. 7 (c)). Because the critical stress for the (001) compound twinning of B19′-NiTi is insensitive of testing temperature [21], the twinning-detwinning deformation is enhanced when the yield stress increases with decreasing testing temperature, resulting in the total recovery strain slightly increasing with decreasing testing temperature.

4. Conclusion

In summary, we proposed a design concept that true elastic deformation and reversible twinning-detwinning deformation run in parallel for developing the bulk metallic materials with ultra-large linear elasticity over a wide temperature range. By engineering the residual internal stress to realize the concurrency of true elastic deformation and twinning-detwinning deformation, we developed a bulk nanocrystalline NiTi that possesses an ultra-large linear elastic strain up to 5.1 % and a high yield stress of 2.16 GPa over a wide temperature range of 270 °C (from -197 °C to 70 °C). Besides, we reveal the effects of grain size and operating temperature on the ultra-large linear elasticity of the NC-NiTi.

Acknowledgments

This work was supported by the National Key R&D Program of China (No. 2018YFB1105100), the National Natural Science Foundation of China (Nos. 51971244 and 51731010), the Science Foundation of China University of Petroleum, Beijing (No. 2462018BJC005), the Pre-research Program of Frontier Science, Ministry of Education (No. 6141A020222) and the Research Fund of China Manned Space Engineering (No. 040201). The use of the Advanced Photon Source was supported by the US Department of Energy, Office of Science, and Office of Basic Energy Science (No. DE-AC02-06CH11357).

Appendix A. Supplementary data

Supplementary material related to this article can be found, in the online version, at doi:https://doi.org/10.1016/j.jmst.2020.01.073.

References

[1] L. Lu, Y.F. Shen, X.H. Chen, L.H. Qian, Science 304 (2004) 422–426.
[2] Y.H. Zhao, X.Z. Liao, S. Cheng, E. Ma, Y.T. Zhu, Adv. Mater. 18 (2006) 2280–2283.
[3] Y.M. Wang, E. Ma, Appl. Phys. Lett. 85 (2004) 2750–2752.
[4] Z.Y. Xu, Trans. Nonferrous Met. Soc. China 11 (1) (2001) 1–9.
[5] K. Otsuka, X. Ren, Prog. Mater. Sci. 50 (2005) 511–678.
[6] Y. Tanaka, Y. Himuro, R. Kainuma, Y. Sutou, T. Omori, K. Ishida, Science 327 (2010) 1488–1490.
[7] H. Sehitoglu, C. Efstathiou, H.J. Maier, Y. Chumlyakov, Mech. Mater. 38 (2006) 538–550.
[8] M.L. Young, M.F.X. Wagner, J. Frenzel, W.W. Schmahl, G. Eggeler, Acta Mater. 58 (2010) 2344–2354.
[9] S.J. Hao, L.S. Cui, Y.D. Wang, D.Q. Jiang, C. Yu, J. Jiang, D.E. Brown, Y. Ren,Appl. Phys. Lett. 99 (2011), 024102.
[10] S. Hao, L. Cui, D. Jiang, X. Han, Y. Ren, J. Jiang, Y. Liu, Z. Liu, S. Mao, Y. Wang, Y. Li, X. Ren, X. Ding, S. Wang, C. Yu, X. Shi, M. Du, F. Yang, Y. Zheng, Z. Zhang, X. Li, D.E. Brown, J. Li, Science 339 (2013) 1191–1194.
[11] T. Omori, K. Ando, M. Okano, X. Xu, Y. Tanaka, I. Ohnuma, R. Kainuma, K. Ishida, Science 333 (2011) 68–71.
[12] Y.L. Hao, H.L. Wang, T. Li, J.M. Cairney, A.V. Ceguerra, Y.D. Wang, Y. Wang, D. Wang, E.G. Obbard, S.J. Li, R. Yang, J. Mater. Sci. Technol. 32 (2016) 705–709.
[13] P.R. Thornton, T.E. Mitchell, Philos. Mag. 7 (1962) 361–375.
[14] H. Suzuki, C.S. Barrett, Acta Metall. 6 (1958) 156–165.

[15] W.R. Bin, M.R. Lopez, G.T.G. Iii, D.J. Idar, Mater. Res. Process. Sci. 7 (1997) 523–528.
[16] S.G. Song, G.T. Gray, Acta Metall. Mater. 43 (1995) 2325–2337.
[17] L. Straka, H. Hänninen, O. Heczko, Appl. Phys. Lett. 98 (2011) 7–11.
[18] M. Vronka, H. Seiner, O. Heczko, Philos. Mag. 97 (2017) 1479–1497.
[19] L. Straka, A. Soroka, H. Seiner, H. Hänninen, A. Sozinov, Scr. Mater. 67 (2012) 25–28.
[20] V.A. Lubarda, M.A. Meyers, O. Vohringer, Acta Mater. 49 (2001) 4025–4039.
[21] J. Wang, H. Sehitoglu, Acta Mater. 61 (2013) 6790–6801.
[22] Y.T. Zhu, X.Z. Liao, X.L. Wu, Prog. Mater. Sci. 57 (2012) 1–62.
[23] B.Q. Li, M.L. Sui, B. Li, E. Ma, S.X. Mao, Phys. Rev. Lett. 102 (2009) 1–4.
[24] M. Sakairi, G. Proust, G.C. Kaschner, I.J. Beyerlein, B. Clausen, D.W. Brown, R.J. McCabe, C.N. Tomé, Experiment. Mech. 50 (2010) 125–133.
[25] H.S. Park, K. Gall, J.A. Zimmerman, Phys. Rev. Lett. 95 (2005) 1–4.
[26] S. Li, X. Ding, J. Deng, T. Lookman, J. Li, X. Ren, J. Sun, A. Saxena, Phys. Rev. B-Condens. Matter Mater. Phys. 82 (2010) 1–12.
[27] S. Hu, C.H. Henager, L. Chen, Acta Mater. 58 (2010) 6554–6564.
[28] J. Wang, Z. Zeng, C.R. Weinberger, Z. Zhang, T. Zhu, S.X. Mao, Nat. Mater. 14 (2015) 594–600.
[29] S. Lee, J. Im, Y. Yoo, E. Bitzek, D. Kiener, G. Richter, B. Kim, S.H. Oh, Nat. Commun. 5 (2014) 1–10.
[30] Y. Wang, Z. Che, Y. Wang, Y. Ren, S. Li, G. Liu, Acta Mater. 140 (2017) 168–175.
[31] Y.F. Zheng, B.M. Huang, J.X. Zhang, L.C. Zhao, Mater. Sci. Eng. A 279 (2000) 25–35.
[32] L.C. Zhao, Y.F. Zheng, W. Cai, Intermetallics 13 (2005) 281–288.
[33] T. Birk, S. Biswas, J. Frenzel, G. Eggeler, Shape Mem. Superelasticity 2 (2016) 145–159.
[34] N. Narita, T. Umemoto, J. Takamura, A. Yamamoto, J. Jpn. Metal Soc. 49 (1978) 1190–1199.
[35] W.T. Zheng, A. Li, Q. Jiang, J. Zhao, F.L. Meng, Mater. Lett. 62 (2007) 964–966.
[36] T. Waitz, D. Spišák, J. Hafner, H.P. Karnthaler, Europhys. Lett. 71 (2005) 98–103.
[37] T. Waitz, T. Antretter, F.D. Fischer, N.K. Simha, H.P. Karnthaler, J. Mech, Phys. Solids 55 (2007) 419–444.
[38] K. M, S. J.B, Acta Mater. 48 (2000) 1325–1344.
[39] T. Waitz, Acta Mater. 53 (2005) 2273–2283.
[40] T. Waitz, V. Kazykhanov, H.P. Karnthaler, Acta Mater. 52 (2004) 137–147.
[41] T. Waitz, W. Pranger, T. Antretter, F.D. Fischer, H.P. Karnthaler, Mater. Sci. Eng. A 481–482 (2008) 479–483.
[42] Z. Xiong, Z. Li, Z. Sun, S. Hao, Y. Yang, M. Li, C. Song, P. Qiu, L. Cui, J. Mater. Sci. Technol. 35 (2019) 2238–2242.
[43] S. Miyazaki, S. Kimura, K. Otsuka, Y. Suzuki, Scr. Metall. Mater. 18 (1984) 883–888.
[44] G.J.J. Gao, Y.J. Wang, S. Ogata, Comput. Mater. Sci. 79 (2013) 56–62.
[45] Y. Wang, E. Ma, R.Z. Valiev, Y. Zhu, Adv. Mater. 16 (2004) 328–331.
[46] M.N. Gusev, O.P. Maksimkin, F.A. Garner, J. Nucl. Phys. Mater. Sci. Radiat. Appl. 403 (2010) 121–125.
[47] K. Komvopoulos, X.G. Ma, Appl. Phys. Lett. 87 (2005) 1–3.
[48] G. Zadno, T. Duerig, Proc. MRS Int. Meet. Adv. Mater. 9 (1989) 201–206.
[49] S. Hao, L. Cui, D. Jiang, C. Yu, J. Jiang, X. Shi, Z. Liu, S. Wang, Y. Wang, D.E. Brown, Y. Ren,Appl. Phys. Lett. 102 (2013), 231905.
[50] C.R. Rathod, B. Clausen, M.A.M. Bourke, R. Vaidyanathan, Appl. Phys. Lett. 88 (2006) 86–88.
[51] K. Tsuchiya, Y. Hada, T. Koyano, K. Nakajima, M. Ohnuma, T. Koike, Y. Todaka, M. Umemoto, Scr. Mater. 60 (2009) 749–752.